Studies of the Local Conformational Properties of the Cell-Adhesion Domain of Collagen Type IV in Synthetic Heterotrimeric Peptides†

Barbara Saccà, Stella Fiori, and Luis Moroder*

Max-Planck-Institute for Biochemistry, Am Klopferspitz 18A, D-82152 Martinsried, Germany

Received November 25, 2002; Revised Manuscript Received February 6, 2003

ABSTRACT: Collagen type IV is a specialized form of collagen that is found only in basement membranes. It is involved in integrin-mediated cell-adhesion processes, and the responsible binding sites for the α1β1 integrin cell receptor have been identified as Asp461 of the two α1 chains and Arg461 of the α2 chain. In the most plausible stagger of native collagen type IV the α2 chain is the tailing one. This has recently been confirmed by the differentiated binding affinities of synthetic heterotrimeric collagen peptides in which the chains were staggered in this native register as well as in the less plausible α1α2α1′ register with an artificial cystine knot. In the present work, two heterotrimeric collagen peptides with chain registers identical to the previous ones were synthesized for fluorescence resonance energy transfer and emission anisotropy measurements, exploiting the native Phe464 in the α2 chain as donor and an Ile467Tyr mutation in the α1′ chain as acceptor fluorophore. This fluorophore pair allowed extraction of more detailed information on the conformational properties of the cell-adhesion epitope incorporated into the central part of the trimeric collagen model peptides. A comparison of the experimentally derived values of the interfluorophore distance and of the orientation factor κ^2 with the values extracted from the molecular model of the trimer in the native stagger confirmed a triple-helical structure of the adhesion-site portion at low temperature. The thermal unfolding of this central domain was specifically monitored by emission anisotropy, allowing unambiguous assignment of the three structural domains of the trimeric collagen molecules detected by microcalorimetry, with the integrin binding site as the portion of weakest triple-helical stability flanked by two more stable triple-helical regions. The results are consistent with the picture of a conformational microheterogeneity as the responsible property for selective recognition of collagens by interacting proteins.

Collagen type IV is the major structural component of the basement membrane where it provides not only a scaffold for incorporation of other constituents of the tissue but also the binding sites for cell adhesion. In its ubiquitous form, collagen type IV consists of two α1 chains and one α2 chain, and in large part this heterotrimer adopts the collagen characteristic triple-helical fold. In this supercoiled structure each single chain is folded into a left-handed poly-Pro-II helix, and the three chains intertwine with a one-residue shift into the right-handed triple-helical coiled coil (*1*−*3*). Because of this one-residue shift the spatial display of the side chains of single residues responsible for recognition by interacting proteins is strongly affected by the stagger of the three chains, in which the α2 chain can be the leading, the middle, or the tailing chain.

The α1β1 integrin binding site of collagen type IV has been identified in the CNBr-derived triple-helical fragment CB3[IV] of collagen type IV and consists of Arg461 within the α2 and Asp461 located on the two α1 chains (*3*, *4*). Exploiting the Phe473 residues of the α1 chains and Trp479 of the α2 chain as the fluorescent donor/acceptor pairs, Golbik et al. (*5*) succeeded by fluorescence resonance energy transfer (FRET)[1] and fluorescence polarization experiments to identify the native stagger of collagen type IV with α2 as the tailing chain. This was accomplished by comparing the experimental values of the interchromophore distance *R* and the orientation factor κ^2 with the ones calculated according to different triple-helical models. This stagger was further confirmed in our laboratory by comparing the binding affinities of α1β1 integrin to synthetic heterotrimeric collagen model peptides (*6*) which contain the sequence portion 457−468 of the cell-adhesion epitope of collagen type IV (*7*) and which were selectively assembled via artificial cystine knots into the two staggers shown in Figure 1 for the trimers A and B (*8*). The trimer A contains the α2 chain as the middle and the trimer B as the tailing chain. Since a triple-helical fold of the adhesion epitope of collagen type IV was the prerequisite for α1β1 integrin binding (*7*), the related sequence portions 457−468 of the α1 and α2 collagen chains were extended N- and C-terminally with three and two Gly-Pro-Hyp repeats, respectively. Moreover, in analogy to the cystine knot present in native collagen type IV downstream from the adhesion site, the C-terminal artificial cystine knot was expected to generate a nucleation center for the triple

† This study was supported by the SFB 563 (Grant C4) of the Technical University of Munich.

* To whom correspondence should be addressed. Tel: 49-89-8578-3905. Fax: 49-89-8578-2847. E-mail: moroder@biochem.mpg.de.

[1] Abbreviations: A, acceptor fluorophore; CD, circular dichroism; D, donor fluorophore; DSC, differential scanning calorimetry; FRET, fluorescence resonance energy transfer.

10.1021/bi0206762 CCC: $25.00
Published on Web 03/07/2003

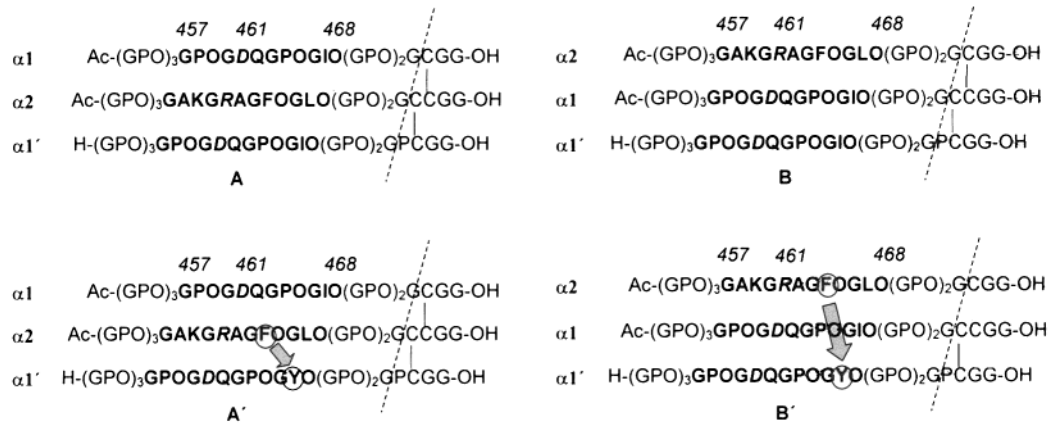

FIGURE 1: Heterotrimeric collagen peptides A, A′, B, and B′. The sequence fragment 457−468 of collagen type IV containing the cell-adhesion epitope for α1β1 integrin is indicated in bold letters whereas the critical R,D,D binding motif in position 461 is indicated in italic letters. Each heterotrimer pair (A/A′ and B/B′) shares the identical amino acid sequence and chain register, being α1α2α1′ for the former and α2α1α1′ for the latter, with the only difference of a single amino acid substitution in the α1′ chain; i.e., Ile467 of the heterotrimers A and B is replaced by a Tyr in the heterotrimers A′ and B′. With this replacement fluorescence energy transfer should take place from Phe464 of the α2 chain (donor) to Tyr467 of the α1′ chain (acceptor) as indicated by the arrow. The alignment of the chains is presented in the order of the synthetic chain assembly, but the dotted line crossing the three chains indicates the stagger of the chains. Correspondingly, the trimers A/A′ contain the α2 chain as the middle chain and the trimers B/B′ as the tailing chain.

helix and thus to stabilize concurrently this fold over the entire heterotrimers (*8*).

The observed higher binding affinity of the integrin receptor for the triple-helical trimer B with the α2 chain as the tailing chain was attributed mainly to the correct spatial display of the involved amino acid residues in this chain alignment. However, an additional modulation of the recognition process may well derive from a certain degree of flexibility of the triple helix in the adhesion-site region of collagen type IV that allows for a better induced fit into the binding pocket of the α1β1 integrin receptor. This hypothesis of plasticity of the triple-helical structure is supported by the conformational properties of the two heterotrimeric model peptides, which clearly revealed a significantly less stable triple helix for the heterotrimer B as the better integrin ligand than for trimer A (*9*).

To gain more detailed information on the conformational properties of these collagen peptides as mimics of the cell-adhesion site of collagen type IV, in the present study two additional heterotrimers, A′ and B′, were synthesized in the staggers of the parent trimers A and B, respectively, as shown in Figure 1. These trimers still contain the sequence portion 457−468 of collagen type IV with the native Phe residue in position 464 of the α2 chain but, in addition, an Ile467Tyr replacement in the α1′ chain to generate a donor−acceptor pair for FRET experiments. As previously observed for the trimers A and B (*8*, *9*), the overall triple-helical fold of the two new model peptides is strongly affected by the chain register. Using both differential scanning calorimetry (DSC) and FRET experiments, regions of different intrinsic structural stability were identified with the adhesion site exhibiting the highest degree of plasticity.

EXPERIMENTAL PROCEDURES

Synthesis of the Heterotrimers A′ and B′. The syntheses of the heterotrimeric collagen peptides A and B (Figure 1) used for comparative experiments were reported previously (*8*). The heterotrimers A′ and B′ (Figure 1) share the identical amino acid composition and chain alignments of the parent trimers with only the Ile residue in position 467 of the α1′ chain being replaced by a Tyr residue. The single peptide chains were synthesized and then assembled into the α1α2α1′ (A′) and α2α1α1′ (B′) registers by adopting the identical procedures as reported for the preparation of the analogous heterotrimers A and B (*8*).

(A) α1′(StBu) A′/B′ [H-Gly-(Pro-Hyp-Gly)$_4$−Asp-Gln-Gly-Pro-Hyp-Gly-Tyr-Hyp-Gly-(Pro-Hyp-Gly)$_2$-Pro-Cys(StBu)-Gly-Gly-OH]: yield, 5.6%; RP-HPLC, t_R 7.68 min; MALDI-TOF MS, m/z = 2982.1 [M$^+$]; M_r = 2982.2 calcd for $C_{129}H_{185}N_{33}O_{45}S_2$; amino acid analysis, Asp 0.96 (1), Cys 0.96 (1), Glu 1.00 (1), Gly 11.89 (12), Hyp 7.80 (8), Tyr 1.02 (1), Pro 6.93 (8); peptide content, 82.4%.

(B) α1′(SH) A′/B′: yield, quantitative; RP-HPLC, t_R 6.62 min; MALDI-TOF MS, m/z = 2894.2 [M$^+$]; M_r = 2894.2 calcd for $C_{125}H_{177}N_{33}O_{45}S_1$.

(C) α1α2α1′ Heterotrimer A′: yield, 25%; RP-HPLC, t_R 7.16 min; amino acid analysis, Ala 2.26 (2), Arg 1.00 (1), Asp 2.00 (2), Cys 3.83 (4), Glu 2.08 (2), Gly 36.58 (36), Hyp 22.06 (23), Ile 0.80 (1), Leu 1.04 (1), Lys 1.04 (1), Phe 1.09 (1), Pro 18.27 (20), Tyr 1.10 (1); peptide content, 58.9%.

(D) α2α1α1′ Heterotrimer B′: yield, 31%; RP-HPLC, t_R 6.85 min; amino acid analysis, Ala 2.13 (2), Arg 1.06 (1), Asp 1.87 (2), Cys 4.25 (4), Glu 1.98 (2), Gly 36.84 (36), Hyp 23.97 (23), Ile 0.85 (1), Leu 1.15 (1), Lys 1.20 (1), Phe 1.00 (1), Pro 19.91 (20), Tyr 0.93 (1); peptide content, 91.8%.

CD Measurements. The CD spectra were recorded on a Jasco J-715 spectropolarimeter equipped with a thermostated cell holder and connected to a data station for signal averaging and processing. All spectra were recorded in the range 190−250 nm, employing quartz cuvettes of 0.1 cm optical path length. The spectra were recorded on peptide solutions preequilibrated at 4 °C for at least 12 h at a concentration of 3×10^{-5} M in Tris buffer (50 mM Tris·HCl, pH 7.4, 50 mM NaCl, 10 mM $CaCl_2 \cdot 2H_2O$). The concentrations were determined by weight and peptide content as obtained from the quantitative amino acid analysis of the peptides. The thermal denaturation curves were monitored on the same peptide solutions following the change in intensity of the CD signal at 222 nm versus the

temperature, in the range 4−70 °C with a heating rate of 0.2 °C/min.

DSC Measurements. The temperature dependence of the partial heat capacity was determined on a VP-DSC microcalorimeter from MicroCal (Northampton, MA) equipped with a cell feedback network and two fixed-in-place cells with effective volumes of ca. 0.5 mL. The measurements were accomplished on peptide solutions of 10^{-4} M concentration in water and preequilibrated at 4 °C for at least 12 h. The thermal denaturation and renaturation curves were recorded as a variation of the heat capacity (C_p) versus the temperature in the range 4−70 °C, using a scan rate of 0.2 °C/min. Data analysis was performed with the Origin software modified for microcalorimetric applications (MicroCal, Northampton, MA) using the *non-two-state* transition model (*2*).

FRET Measurements. Fluorescence emission spectra were acquired on a LS 50B Perkin-Elmer luminescence spectrometer equipped with a fluorescence polarization unit and a RK 20 Lauda thermostat controlled by a FL WinLab software version 2.01 from Perkin-Elmer. The experiments were carried out on peptide solutions preequilibrated at 4 °C for at least 12 h, at a concentration of 10^{-4} M in water, using QS 1000 quartz cells (Hellma GmbH, Badern) of 0.2 cm inside width. Excitation of the donor fluorescence (Phe residue) was performed at 260 nm, and the emission spectra were recorded in the range 270−300 nm, using a slit of 2.5 nm for both excitation and emission monochromators and a scan speed of 200 nm/min. The average of 10 scans is reported.

(A) Determination of the Energy Transfer Efficiency. Steady-state energy-transfer measurements were performed by comparing the emission fluorescence intensities of the heterotrimers A′ and B′, containing the donor−acceptor pair, to those of the heterotrimers A and B, respectively, containing only the donor fluorophore. The extent of donor quenching due to the acceptor was estimated using the "area under the curve" method (*10*). The experiments were repeated three times under the same conditions, and the mean value of E was determined.

(B) Calculation of the Fluorophore Internal Distance. The donor−acceptor distance R was determined according to the equation (*11*):

$$E = {R_0}^6/({R_0}^6 + R^6) \qquad (1)$$

where E is the energy transfer efficiency experimentally determined by steady-state measurements and R_0 is the Förster or critical transfer distance, which is defined as the distance at which the energy transfer E is 50% efficient.

(C) Calculation of R_0. The Förster distance R_0 is a chromophore pair dependent parameter which is related to the spectroscopic properties and relative orientation of the donor and acceptor in a specific environment according to the equation:

$$R_0 = (9.789 \times 10^{-5})(\kappa^2 n^{-4} \Phi_D J_{AD})^{1/6} \qquad (2)$$

where n is the refractive index of the solvent, Φ_D is the quantum yield of the donor, J_{AD} is the spectral overlap integral between the donor and the acceptor, and κ^2 is the orientation factor. A first calculation of the Förster distance R_0 was performed by substituting in eq 2 the literature values of the parameters which describe the donor−acceptor pair under the experimental conditions (*12*). Accordingly, R_0 was calculated for three different values of the donor quantum yield ($\Phi_D = 0.05$, 0.10, and 0.20), using the refractive index n of water ($n = 1.5$) and the overlap integral J_{AD} for the Phe-Tyr pair in water at low temperature ($J_{AD} = 4.0 \times 10^{-16}$ M^{-1} cm^6). The value of $^2/_3$ was initially applied for the orientation factor κ^2 assuming a random distribution of the dipole orientations (*13*, *14*), and the separation distance R between the donor and the acceptor was calculated according to eq 1. Successively, correction of the orientation factor was performed by anisotropy measurements, and effective values of the Förster and interchromophore distances were determined.

Fluorescence Anisotropy Measurements. The emission anisotropy measurements were accomplished on the same instrument used for the FRET experiments and were performed on peptide solutions of 10^{-5} M concentration in water using quartz cells of 1 cm inside width. Excitation of the Phe (donor) fluorescence was performed at 260 nm, and emission of the Tyr (acceptor) was monitored at 305 nm. After the G-factor for the respective wavelength pair was determined, the emission anisotropy was measured at 4 °C using a slit of 15 nm for both the excitation and the emission monochromators, a duration time of 180 s, and a data pitch of 0.4 s. The average value of three measurements is reported. Finally, the thermal denaturation of the heterotrimer B′ was monitored by following the change in intensity of the emission anisotropy signal at 305 nm versus the temperature, in the range 4−70 °C, using a band-pass of 15 nm, a data interval of 4 s, and a heating rate of 0.2 °C/min.

(A) Calculation of the Effective Orientation Factor. The correlation between the effective orientation factor (κ^2_{eff}) and emission anisotropy (r) is described by the equation:

$$\kappa^2_{eff} = (2 + 5r)/3 \qquad (3)$$

assuming that the observed anisotropy is not affected by other depolarizing processes. In this correlation the mathematical model developed by Dale and Eisinger was used, as it best fits to the molecular properties of the triple helix (*15*). However, the dynamic situation during energy transfer is not considered in order to avoid a complex mathematical treatment which goes beyond our purposes (see Supporting Information). Therefore, within the limits of these reasonable approximations, one can calculate the effective orientation factor from eq 3, and by substituting this value in eq 2, the corrected value of the Förster distance is obtained. Consequently, a better estimate of the spatial distance between the donor and the acceptor can be provided from eq 1.

Molecular Dynamics. MD calculations were performed on Silicon Graphics O2 R5000 and Octane R10000 computers (Silicon Graphics Inc., Mountain View, CA) with the InsightII program package (Accelrys, San Diego, CA). An explicit solvent model was employed for simulation of the aqueous system by using a 110 × 45 × 45 TIP3 water box (*16*). The starting 3D coordinates of the $(Gly\text{-}Pro\text{-}Hyp)_{10}$ collagen structure (*17*) were taken from the Brookhaven Protein Data Bank, whereby the necessary sequence modifications to create the trimers A′ and B′ were done without any change of the backbone atom positions. The heterotri-

mers A′ and B′ were embedded in water, and the energy of the system was first minimized while maintaining all atom coordinates fixed. The simulations were performed by heating stepwise from a starting temperature of 100 K to a final temperature of 277 K without constraints except for the planarity of the peptide group (force constant of 100.0 kcal mol^{-1} $Å^{-2}$). A total of 200 structures were generated at the final temperature over a production period of 200 ps. The minimal and maximal distances between the aromatic ring centers of Phe464 (α2 chain) and Tyr467 (α1′ chain) were taken from the last MD structure. Both fluorophore side chains were allowed to rotate around the $C^{\alpha}-C^{\beta}$ axis describing cones whose apexes are occupied by the C^{β} atoms. The extracted distances for the trimers A′ and B′ are in the range of 9.7−15.2 and 11.1−14.1 Å, respectively.

RESULTS

Design of the Heterotrimers A′ and B′. The dependence of the energy transfer efficiency from the inverse sixth power of the distance between the donor and the acceptor allows use of FRET as a spectroscopic ruler for estimating distances in biomolecular systems (*18*). To apply this technique, a donor−acceptor fluorophore pair is required. Moreover, for energy transfer to occur, some conditions must be satisfied, such as a sufficient overlap between the emission spectrum of the donor and the absorption spectrum of the acceptor, an appropriate relative distance between the two fluorophores, and a favorable dipole orientation. Concerning the donor−acceptor distance, experiments with model systems have shown that the Förster theory (*11*) can be applied in reliable manner whenever the donor and the acceptor are within a factor of 2 of the critical distance ($R \leq 2R_0$), which can range from 10 to 100 Å. Taking into account these prerequisites as well as the necessity of minimal changes in the natural sequence of the adhesion epitope, the Phe residue in position 464 of the α2 chain was taken as the donor, although being a poor fluorophore. Since previous conformational analysis had clearly confirmed an overall triple-helical fold of both the trimer A and B of Figure 1 (*8*, *9*), the Ile residue in position 467 of the α1′ chain at the edge of the adhesion epitope appeared to be in favorable distance for replacement by a Tyr residue to generate the fluorophore acceptor. In fact, the native Trp479 exploited by Golbik et al. (*5*) for the FRET experiments is located too downstream of the adhesion site for use in the model peptides. Moreover, replacement of Ile467 with a Trp residue as the better fluorophore would severely hamper the assembly of the trimers by the cysteine chemistry applied because of the required use of sulfenyl chlorides in the regioselective cysteine pairing procedures (*19*). Correspondingly, even a substitution of both the Phe and Ile residues by a Tyr and Trp, respectively, to generate a more efficient donor−acceptor pair was not feasible.

Dichroic Properties of the Heterotrimers A′ and B′. The CD spectra of the heterotrimers A′ and B′ in aqueous buffer are typical of triple-helical collagenous peptides, and the related parameters are reported in Table 1 in comparison to those of the parent heterotrimers A and B. Taking into account the effects on the triple-helix stability caused by amino acid substitutions of Pro and/or Hyp in the typical collagen Gly-Pro-Hyp triplet, as determined by host−guest studies on model collagenous peptides (*20*, *21*), a lower thermal stability of the trimers A′ and B′ was predicted for the Ile467Tyr replacement. However, the related Rpn values would suggest a higher triple-helix content and/or stability induced by this single residue mutation. In full agreement with this observation were the enhanced melting temperatures of the heterotrimers A′ and B′ as extracted from thermal denaturation curves monitored at 222 nm (Table 1); but again a strong effect of the chain register was observed, which is consistent with that reported for the trimers A and B (*8*, *9*), i.e., a difference of about 10 °C. The sigmoidal traces of the thermal excursions for both trimers (data not shown) are consistent with a highly cooperative transition that supports a triple-helical structure spanning the entire trimers from the C- to the N-terminus.

Table 1: Dichroic Parameters of the Heterotrimeric Collagen Peptides Containing the Adhesion Epitope 457−468 of Collagen Type IV at 3×10^{-5} M Concentration in 50 mM Tris·HCl, 50 mM NaCl, and 10 mM $CaCl_2 \cdot 2H_2O$ (pH 7.4)[a]

collagen peptides	max (λ, θ_R)	min (λ, θ_R)	Rpn[b]	t_m (°C)
heterotrimer A	224, 3831	198, −34317	0.112	42
heterotrimer A′	224, 6373	199, −47250	0.135	44
heterotrimer B	225, 4078	199, −37274	0.109	30
heterotrimer B′	225, 3929	199, −30178	0.131	34
fragment F4 of collagen type IV[c]				50

[a] The CD spectra were recorded at 4 °C after 12 h preequilibration at the same temperature. The thermal denaturation curves were monitored at 222 nm with a heating rate of 0.2 °C/min. [b] Rpn is defined as the absolute value of the ratio between the dichroic intensities of the positive maximum over that of the negative maximum. [c] The fragment F4 of collagen type IV corresponds to the sequence portions 434−516 of the α1 and α2 chains and contains in the central part the α1β1 integrin binding site flanked up- and downstream by a cystine knot (*4*).

Microcalorimetric Measurements. Unfolding and refolding of the heterotrimers A′ and B′ were monitored by DSC, and the corresponding endo- and exotherms are shown in panels a and b of Figure 2. The processes are reversible as confirmed by superimposition of the CD spectra at 4 °C before denaturation and after 12 h equilibration upon renaturation (data not shown). In analogy to the behavior of the parent peptides (*9*), a kinetic hysteresis is observed in the refolding process. Deconvolution analysis of the endo- and exotherms of the two heterotrimers A′ and B′ confirmed the presence of a multidomain conformational organization even in these analogues, and the related parameters are listed in Table 2. In our previous study of the trimers A and B the type of chain alignment was found to affect strongly only the melting temperature of the component with the lowest conformational stability (peak I), while the two more stable domains showed identical t_m values independently of the chain raster (*9*). Within the limits of experimental errors a similar behavior was observed for the analogues A′ and B′. As reported previously (*9*), the most stable structural domain (peak III) of the trimers A and B was assigned to the cystine knot on the basis of comparative analysis with a trimer lacking the cystine connectivities, whereas the other two domains were tentatively assigned in order of increasing thermal stability to the central adhesion epitope (peak I) and the regular (Gly-Pro-Hyp) repeats (peak II), by taking into account the known triple-helix propensities of collagenous sequences. An analogous assignment of the three domains in the trimers A′ and B′ is further supported by the observation that the Ile467Tyr

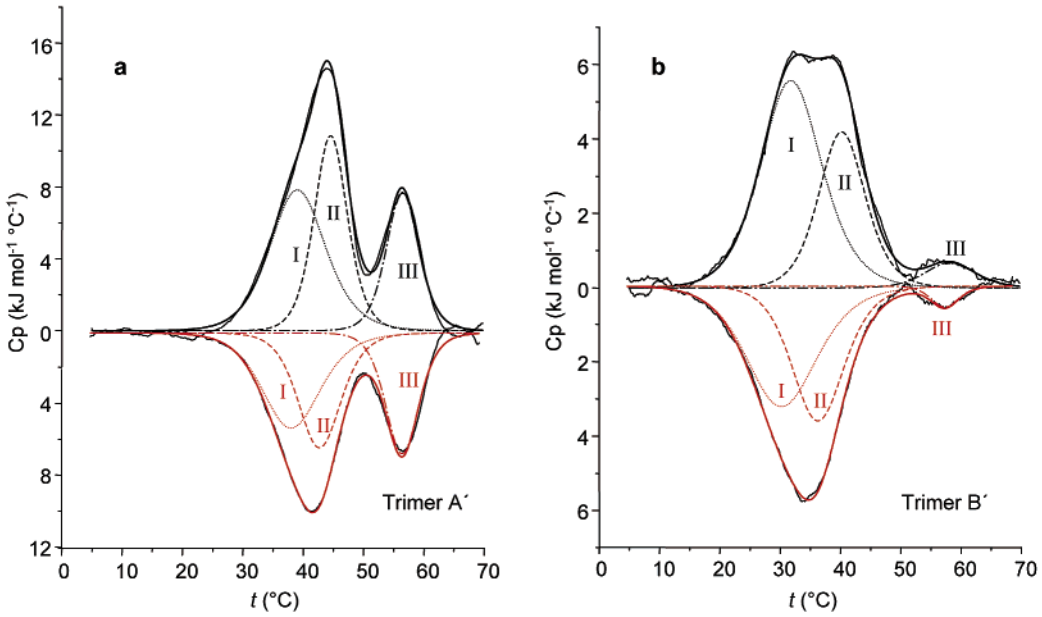

FIGURE 2: Thermal denaturation (black) and renaturation (red) profiles obtained by differential scanning calorimetry of the heterotrimers A′ (left panel) and B′ (right panel) at 8×10^{-5} M concentration in water. A heating rate of 0.2 °C/min was applied in the temperature range from 4 to 70 °C. Deconvolution analysis of both the endotherms and the exotherms led to the identification of three peaks (indicated in Roman numerals) which are associated to three distinct domains within the collagen molecule: I, central adhesion epitope; II, N- and C-terminal (Gly-Pro-Hyp) repeats; III, C-terminal cystine knot (*9*). In the refolding processes the peaks are shifted to lower temperatures and exhibit lower intensities according to the kinetic hysteresis already observed for the parent heterotrimers A and B (*9*).

Table 2: DSC Data of the Heterotrimeric Collagen Peptides Containing the Adhesion Epitope of Collagen Type IV at 8×10^{-5} M Concentration in Water[a]

collagen peptide	deconvoluted peak	t_m (°C)	collagen peptide	deconvoluted peak	t_m (°C)
heterotrimer A	I	*38*	heterotrimer A′	I	*39*
	II	44		II	45
	III	57		III	57
heterotrimer B	I	*32*	heterotrimer B′	I	*32*
	II	44		II	41
	III	57		III	58

[a] Deconvolution analysis for the thermal denaturation of the heterotrimers allowed identification of three peaks which were assigned, in order of thermal stability, to the central adhesion epitope (peak I), Gly-Pro-Hyp triple-helical repeats (peak II), and the C-terminal cystine knot (peak III). The t_m related to the three cooperative units are reported, and the ones corresponding to the central adhesion domain are indicated in italics.

mutation located in the cell-adhesion epitope is not affecting the difference in thermal stability between the two staggers (about 7 °C in favor of trimers A/A′ vs B/B′). Within the experimental errors, the t_m value of peak I in each pair of analogous trimers is substantially constant, i.e., 39 °C for the trimers A/A′ and 32 °C for the trimers B/B′ (Table 2).

FRET Measurements. The relatively low intensity of Phe fluorescence in the near-UV makes this chromophore not ideal for FRET experiments; however, its intensity was increased by using higher peptide concentrations in aqueous solution (10^{-4} M). Upon excitation of the Phe fluorescence at 260 nm the emission spectra of the heterotrimers A and B were recorded in the 270−300 nm range and compared with the emission spectra of the heterotrimers A′ and B′ under identical experimental conditions (Figure 3). The extent of energy transfer between the fluorophores Phe and Tyr was estimated by using the area under the curve method (*10*) in each heterotrimer pair (A/A′ and B/B′).

As well evidenced by Figure 3A, no energy transfer is taking place in the heterotrimer A′ where the fluorescence emission related to the Phe residue is substantially unaffected by the presence of the Tyr acceptor residue. Conversely, in the heterotrimer B′ (Figure 3B) a significant quenching of the Phe fluorescence is observed as a result of energy transfer to the Tyr acceptor with an efficiency of ca. 58%. Although the partial overlap of the fluorescence emission spectra of Phe ($\lambda_{max} = 285$ nm) and Tyr ($\lambda_{max} = 305$ nm) may cause possible errors in extracting the intramolecular Phe/Tyr distance in the heterotrimer B′, the value of 58% energy transfer efficiency was used for a first estimation of this distance applying eq 1 for different values of the donor quantum yield (Table 3). In these calculations the relative orientation between donor and acceptor was considered dynamically averaged to a random situation expressed by the orientation factor $\langle\kappa^2\rangle = {}^2/_3$. Since the energy transfer efficiency is strongly affected by the relative fluorophore orientation, a more accurate estimation of the κ^2 factor was derived from anisotropy measurements (*22*, *23*).

Emission Anisotropy Measurements. Low temperature (4 °C) and low peptide concentration (10^{-5} M) were used to minimize the effect of rotational diffusion and intermolecular energy transfer, respectively. Indeed, both of these processes result in additional angular displacement of the emission oscillator and hence in lower anisotropies. After determination of the *G*-factor for the Phe/Tyr pair of fluorophores ($G = 0.754$), the emission anisotropy r of Tyr was measured at 305 nm upon excitation of the Phe fluorescence at 260 nm. A mean value of $r = 0.053$ was derived, and calculation of the effective orientation factor for the two fluorophores in the heterotrimer B′ was performed by applying eq 3. The effective values of R_0 and R calculated from κ^2_{eff} are shown in Table 3. The differences between the two sets of data, i.e., for $\langle\kappa^2\rangle = {}^2/_3$ and $\kappa^2_{eff} = 0.755$, can be considered

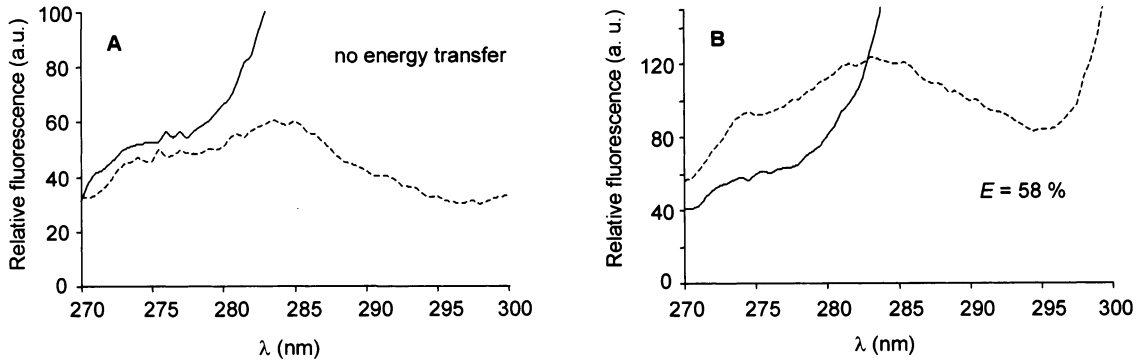

FIGURE 3: Fluorescence emission spectra of the heterotrimers A (---) and A′ (—) (left panel) and B (- - -) and B′ (—) (right panel) at 4 °C and 10^{-4} M concentration in water upon excitation of the Phe fluorescence at 260 nm. In the heterotrimer A′ (left panel) the interchromophore distance does not allow for an efficient energy transfer to occur, whereas the arrangement of the chains in the heterotrimer B′ (right panel) allows an energy transfer efficiency of ca. 58%, which was calculated according to the area under the curve method (*10*).

Table 3: Estimated Values of the Förster Distance R_0 and Separation Distance R between Phe464 of the α2 Chain and Tyr467 of the α1′ Chain for the Heterotrimer B′ at 4 °C and 10^{-4} M Concentration in Water[a]

	R_0 (Å)[b]			R (Å)[c]		
	$\Phi_D =$ 0.05	$\Phi_D =$ 0.10	$\Phi_D =$ 0.20	$\Phi_D =$ 0.05	$\Phi_D =$ 0.10	$\Phi_D =$ 0.20
$\langle\kappa^2\rangle = {}^2/_3$	11.6	12.7	14.2	10.9	12.0	13.4
$\kappa^2_{eff} = 0.755$[d]	11.8	13.0	14.5	11.1	12.3	13.7

[a] Both values were calculated for different donor quantum yields (Φ_D) and for dynamically averaged $\langle\kappa^2\rangle$×98 and effective (κ^2_{eff}) orientation factors. [b] Förster distance calculated according to eq 2, where n is the refractive index of water ($n = 1.5$) and J_{AD} is the overlap integral for the donor−acceptor pair ($J_{AD} = 4.0 \times 10^{-16}$ M^{-1} cm^6) (*12*). [c] Estimated Phe−Tyr distance calculated from FRET measurements according to eq 1 with $E = 58\%$. [d] Effective orientation factor calculated from anisotropy measurements according to eq 3 with $r = 0.053$.

negligible, allowing an approximation of the relative dipole orientation between the two fluorophores to a randomly averaged situation. In fact, the experimental R values of 11.1−13.7 Å are consistent with those derived from the modeling experiments for trimer B′ in triple helix (11.1−14.1 Å) where the aromatic rings of the two fluorophore side chains were allowed to rotate freely around the $C^{\alpha}-C^{\beta}$ axis (Figure 4).

Thermal Denaturation of the Heterotrimer B′ Monitored by Emission Anisotropy Measurements. The changes in intensity of the emission anisotropy signal of the heterotrimer B′ at 305 nm were monitored in function of temperature and plotted as fractional values. The resulting sigmoidal melting curve (Figure 5) is indicative of a cooperative conformational transition characterized by a t_m value of 32 °C and involving the topochemical environment of the spectral probes, i.e., the cell-adhesion epitope of trimer B′.

DISCUSSION

Generally, by monitoring the thermal denaturation of native collagens and related fragments with CD, monophasic cooperative transitions are observed unless triple-helical segments are interrupted by noncollagenous regions as in the case of collagen type IV and related fragments for which multiphasic transition profiles were observed (*7*, *24*, *25*). Since in cooperative systems, such as the triple helix, the total stabilizing energy is made up of the contributions of all tripeptide units, it is difficult to identify in single triple-helix regions of different intrinsic stability. In fact, the thermal denaturation curves of the heterotrimers A and B as well as of their analogues A′ and B′, as monitored by CD, are monophasic and characterized by melting temperatures that reflect a surprisingly strong effect of the chain register on the overall triple-helix stability (Table 1: A vs B and A′ vs B′). In addition, even the single Ile467Tyr replacement is affecting the overall triple-helix stability (Table 1: A vs A′ and B vs B′).

However, by monitoring denaturation and refolding of the heterotrimers with DSC, the overall triple-helical structure of the heterotrimers could be resolved into domains of different intrinsic stabilities. In analogy to the results obtained with the trimers A and B (*9*), deconvolution of the denaturation curves of the trimers A′ and B′ clearly revealed the presence of three structural domains of different thermal stabilities. Within the experimental errors, the melting temperatures of the domains II and III are minimally affected both by the register of the chains and by the replacement of Ile467 with Tyr in the adhesion epitope (Figure 2 and Table 2). Conversely, the thermal stability of domain I is strongly affected by the chain register with an increase of its t_m value by 6 and 7 °C in favor of the trimers A and A′, while it is substantially unaffected by the single amino acid mutation.

In the present study the Ile467Tyr substitution was performed to generate a fluorophore pair suitable for FRET experiments with minimal changes to the native sequence of the cell-adhesion epitope of collagen type IV. According to the Förster theory, the most efficient fluorescence energy transfer is expected only when the donor and the acceptor fluorophore are within the critical distance R_0. Its effective value was found to range between 11.8 and 14.5 Å (Table 3) as determined by anisotropy measurements on our fluorophore pair system. Therefore, from the measurements of the energy transfer efficiency (Figure 3), it can be derived that the Phe/Tyr distance in the spatial display imposed by the α1α2α1′ register of the heterotrimer A′ does not satisfy the optimal range imposed by the Förster distance. Conversely, in the α2α1α1′ register of the heterotrimer B′ the same pair of residues has to be arranged in a way such that their relative distance is within the optimal Förster distance R_0, allowing an efficient energy transfer. These results are fully supported by the modeling experiments. Indeed, the distance between the two fluorophores in the molecular model of the heterotrimer A′ was found to be in the range

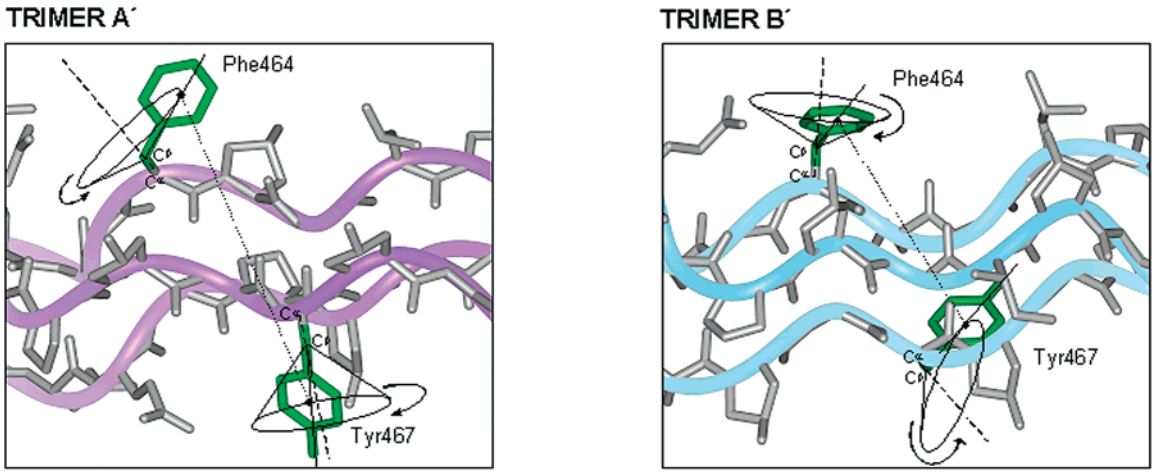

FIGURE 4: Depiction of the relative orientation of the fluorophore side chains in the two different chain alignments of the heterotrimers A′ and B′ (left and right panels, respectively). The aromatic rings of the donor−acceptor pair involved in the energy transfer process are shown in green and correspond to Phe464 of the α2 chain (donor) and Tyr467 of the α1′ chain (acceptor). In ideal conditions both fluorophore side chains are allowed to rotate around an axis given by the C^{α} and C^{β} atoms and describing a cone whose apex is occupied by the C^{β} atoms. The extracted distances for the trimers A′ amd B′ are in the range of 9.7−15.2 and 11.1−14.1 Å, respectively.

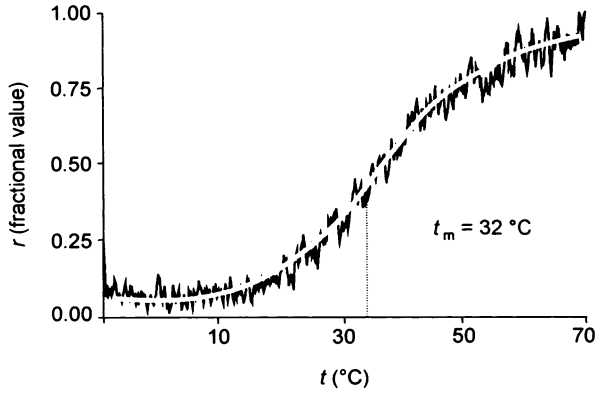

FIGURE 5: Thermal denaturation of the heterotrimer B′ at 10^{-5} M concentration in water monitored by changes in emission anisotropy intensity at 305 nm versus increasing temperature (4−70 °C) with a heating rate of 0.2 °C/min. A melting temperature of 32 °C was derived.

of 9.7−15.2 Å, which is about 50% broader than the optimal Förster distance. Therefore, in this chain register only half of the possible distances determined by modeling can generate an efficient energy transfer. Moreover, at small distance values the two fluorophores are displayed unfavorably with the aromatic rings pointing toward the inner part of the triple helix. Consequently, in the heterotrimer A′ the rotation of the two fluorophores around the $C^{\alpha}-C^{\beta}$ axis will be restricted to a narrow cone, allowing only higher distance values which are far from the optimal R_0 value, thus providing a reasonable explanation for the lack of FRET in this chain arrangment. On the other hand, the distance between the two fluorophores as derived from the molecular model of the heterotrimer B′ was found to be in the range 11.1−14.1 Å, which is included within the Förster value and therefore accounts for the energy transfer efficiency of about 58%.

In the calculation of the internal distance *R*, a first estimate of R_0 was taken, assuming a random distribution of the mutual orientations of the probes corresponding to an orientation factor $\langle\kappa^2\rangle = {}^2/_3$ (*13*, *14*) (Table 3). If the donor−acceptor pair adopts a particular orientation such that their orientation factor is far off from the dynamically averaged value of $^2/_3$, then the calculated distance would be wrong. Since this is particularly the case for viscous solutions or for sterically hindered fluorophores attached to large, slowly rotating substrates, such as collagen-like molecules, an estimate of the true value of the orientation factor was required. Although at present there is no way to measure κ^2, apart from the X-ray structure, it is possible at least to set limits on its value, which in turn sets limits on the range of possible donor−acceptor distances. These limits can be determined by anisotropy measurements (*22*, *23*), multiple donor−acceptor pairs (*26*), and statistical interpretation of the results (*27*). In the present study, emission anisotropy measurements were used to calculate the effective value of the Förster distance R_0 in the target peptides. As reported in Table 3, the difference between the two sets of data can be considered almost negligible.

A comparison of the experimentally derived values for the distance *R* and for the orientation factor κ^2 with the values extracted from the molecular model of trimer B′ confirmed a triple-helical structure of the adhesion-site portion. When the temperature is increased, the emission anisotropy changes (Figure 5), a fact that is correlated with the fluorophores Phe and Tyr located in two chains in the central part of the trimer B′ and should reflect only unfolding of this portion of the collagen peptide. The melting temperature of this portion of the triple helix is 32 °C, a value which fully agrees, at least within the experimental errors of such measurements, with the melting temperature of the deconvoluted peak I of the trimer B′ endotherm (Figure 2B and Table 2). These findings fully support an assignment of this peak to the adhesion epitope of the collagenous trimers.

In conclusion, the synthetic heterotrimer B with its high affinity for the α1β1 integrin is folded into a triple-helical structure of local conformational heterogeneity. In fact, it consists of regions of different intrinsic stabilities with the adhesion epitope of collagen type IV exhibiting the strongest plasticity as possibly required for an optimal fitting to the receptor binding pocket. In native collagen type IV up- and downstream of the adhesion site cystine knots are present which are expected to significantly stabilize the triple-helical structure (*7*), as mimicked in our model peptides by the

C-terminal cystine knot and the additional Gly-Pro-Hyp repeats as the most ideal triplets for induction of the collagen fold. The intrinsic low conformational stability of the adhesion epitope embedded into the two more stable flanking triple helices may possibly reflect a more general characteristic of natural collagens in which sequence- and raster-dependent local plasticity may serve to overcome the limitations imparted by a compact triple helix on the complementarity of protein−collagen binding domains in physiologically important processes. In fact, a partly unfolded triple helix has been already suggested as responsible for recognition of collagen type I by collagenases (*28*) as well as for binding of collagen type IV to melanoma cell CD44−chondrotin sulfate proteoglycan receptors (*29*).

ACKNOWLEDGMENT

The authors gratefully acknowledge the excellent technical assistance of Mrs. Elisabeth Weyher.

SUPPORTING INFORMATION AVAILABLE

Calculation of the orientation factor from anisotropy measurements. This material is available free of charge via the Internet at http://pubs.acs.org.

REFERENCES

1. Fraser, R. D. B., MacRay, T. P., and Suzuki, E. (1979) *J. Mol. Biol. 129*, 463−481.
2. Privalov, P. L. (1982) *Adv. Protein Chem. 35*, 1−104.
3. Beck, K., and Brodsky, B. J. (1998) *Struct. Biol. 122*, 17−29.
4. Kern, A., Eble, J., Golbik, R., and Kühn, K. (1993) *Eur. J. Biochem. 215*, 151−159.
5. Golbik, R., Eble, J. A., Ries, A., and Kühn, K. (2000) *J. Mol. Biol. 297*, 501−509.
6. Saccà, B., Sinner, E. K., Kaiser, J. T., Lübken, C., Eble, J. A., and Moroder, L. (2002) *ChemBioChem 3*, 904−907.
7. Eble, J. A., Golbik, R., Mann, K., and Kühn, K. (1993) *EMBO J. 12*, 4795−4802.
8. Saccà, B., and Moroder, L. (2002) *J. Pept. Sci. 8*, 192−204.
9. Saccà, B., Renner, C., and Moroder, L. (2002) *J. Mol. Biol. 324*, 309−318.
10. Lin, T. I., and Dowben, R. M. (1983) in *Excited States of Biopolymers* (Steiner, R. F., Ed.) pp 59−115, Plenum Press, New York.
11. Förster, T. (1948) *Ann. Phys. (Berlin) 2*, 55−75.
12. Eisinger, J., Feuer, B., and Lamola, A. A. (1969) *Biochemistry 8*, 3908−3915.
13. Förster, T. (1951) *Fluoreszenz Organischer Verbindungen*, Vandenhoeck & Ruprecht, Göttingen.
14. Förster, T. (1966) *Modern Quantum Chemistry*, Academic, New York.
15. Dale, R. E., and Eisinger, J. (1974) *Biopolymers 13*, 1573−1605.
16. Jorgensen, W. L., Chandrasekhar, J., Madura, J. D., Impey, R. M., and Klein, M. L. (1983) *J. Chem. Phys. 79*, 926−935.
17. Fraser, R. D., MacRae, T. P., and Suzuki, E. (1979) *J. Mol. Biol. 129*, 463−481.
18. Stryer, L. (1978) *Annu. Rev. Biochem. 47*, 819−846.
19. Ottl, J., and Moroder, L. (1999) *Tetrahedron Lett. 40*, 1487−1490.
20. Ramshaw, J. A. M., Shah, N. K., and Brodsky, B. (1998) *J. Struct. Biol. 122*, 86−91.
21. Persikov, A. V., Ramshaw, J. A. M., Kirkpatrick, A., and Brodsky, B. (2000) *Biochemistry 39*, 14960−14967.
22. Lakowicz, J. R. (1999) in *Principles of Fluorescence Spectroscopy*, pp 367−394, Plenum Publishers, New York.
23. Dale, R. E., Eisinger, J., and Blumberg, W. E. (1979) *Biophys. J. 26*, 161−193.
24. Engel, J. (1987) in *Collagen as a Food*, pp 145−161, AVI Book, New York.
25. Bächinger, H. P., Fessler, L. I., and Fessler, J. H. (1982) *J. Biol. Chem. 257*, 9796−9803.
26. Matsumoto, S., and Hammes, G. G. (1975) *Biochemistry 14*, 214−224.
27. Hillel, Z., and Wu, C. W. (1976) *Biochemistry 15*, 2105−2113.
28. Fiori, S., Saccà, B., and Moroder, L. (2002) *J. Mol. Biol. 319*, 1235−1242.
29. Malkar, N. B., Lauer-Fields, J. L., Borgia, J. A., and Fields, G. B. (2002) *Biochemistry 41*, 6054−6064.
30. Jablonski, A. (1971) *Bull. Acad. Pol. Sci., Ser. Sci., Math., Astron., Phys. 19*, 171.

BI0206762